Electronic Supplementary Material (ESI) for Journal of Materials Chemistry A.

Electronic Supplementary Information

Functionalised metal-organic frameworks: a novel approach to stabilising single metal atoms

P. Á. Szilágyi, D. M. Rogers, I. Zaiser, E. Callini, S. Turner, A. Borgschulte, A. Züttel, H. Geerlings, M. Hirscher and B. Dam

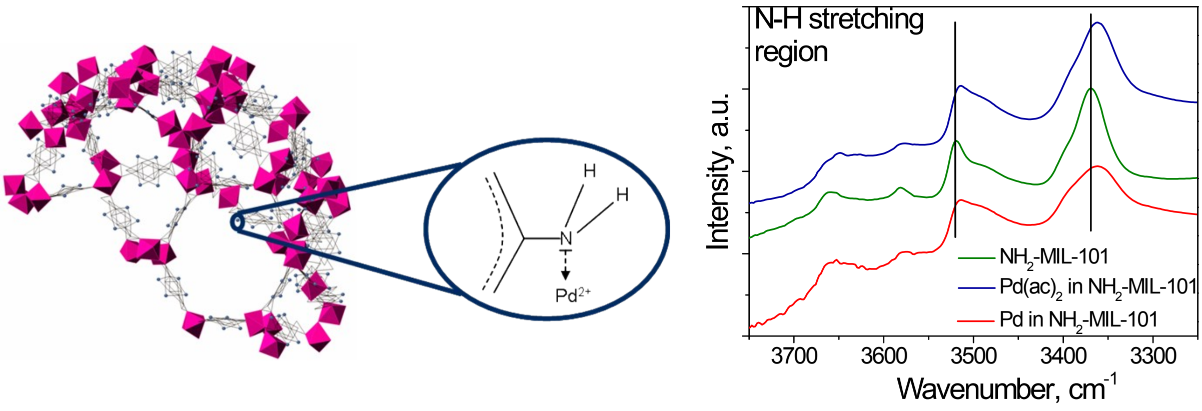

Figure S1 From left to right: half of a large pore of NH_2-MIL-101(Cr) highlighting the specific Pd^{2+}-NH_2 bonding and DRIFT spectrum of the pristine, $Pd(ac)_2$ and Pd containing NH_2-MIL-101(Cr) in the N-H vibration mode region displaying a slight shift due to specific bonding

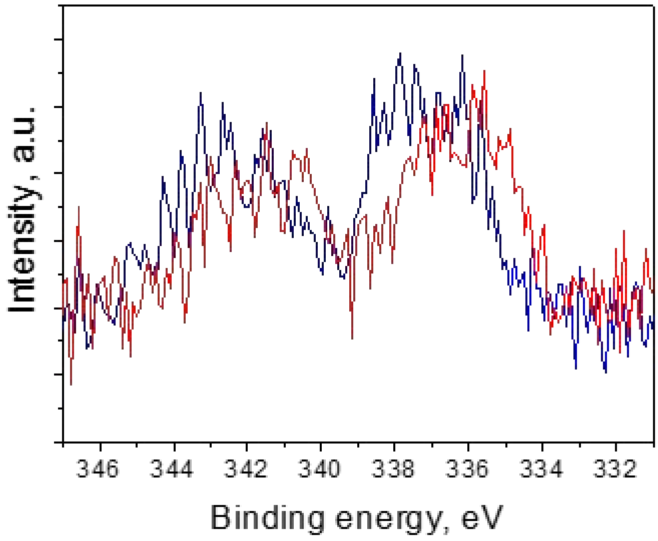

Figure S2 X-ray photoelectron spectra of the $Pd(ac)_2$ precursor (in blue) and the elemental Pd (in red) containing NH_2-MIL-101(Cr)

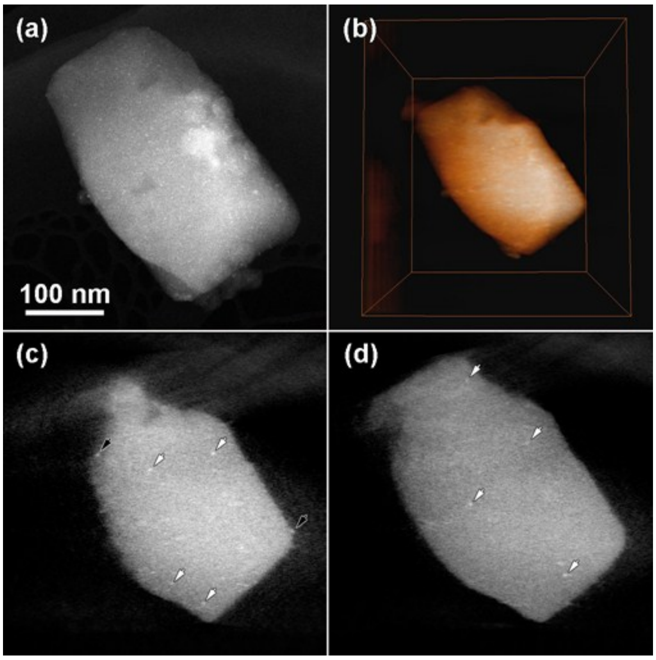

Figure S3 TEM tomography images of the Pd containing NH_2-MIL-101(Cr), **a)** HAADF-STEM image taken at 0 degrees tilt; **b)** reconstructed volume; **c)** and **d)** ortho-slices through the reconstructed volume; some particles are present at the surface of the MOF host (examples shown in black arrows), others are clearly embedded within the host volume (examples shown in white arrows).

These distinctions can be made as particles on the surface appear exposed in certain ortho-slices while embedded particles appear in the centre of the MOF particle in every ortho-slice.

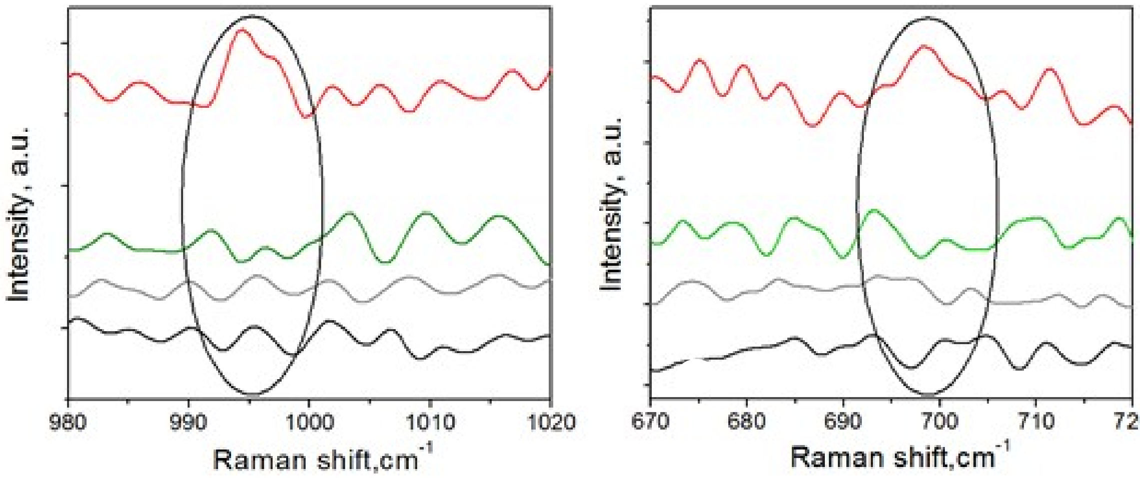

Figure S4 Raman spectra of the Pd containing NH_2-MIL-101(Cr) under vacuum in grey and the pressure cell in black, the pristine NH_2-MIL-101(Cr) in green and the Pd containing NH_2-MIL-101(Cr) in red **c)** under 20 bar hydrogen and **d)** deuterium pressure at ambient temperature

Under 20 bar hydrogen pressure, the appearance of a small peak at 994.5 cm^{-1} can be observed (left). Furthermore, when hydrogen was replaced by deuterium (right), another peak was detected at 698.3 cm^{-1}, representing an isomer shift by a factor of 1.4 (or *ca.* $\sqrt{2}$). Such shift is indicative of the formation of adducts with a hydrogen molecule or an atom.

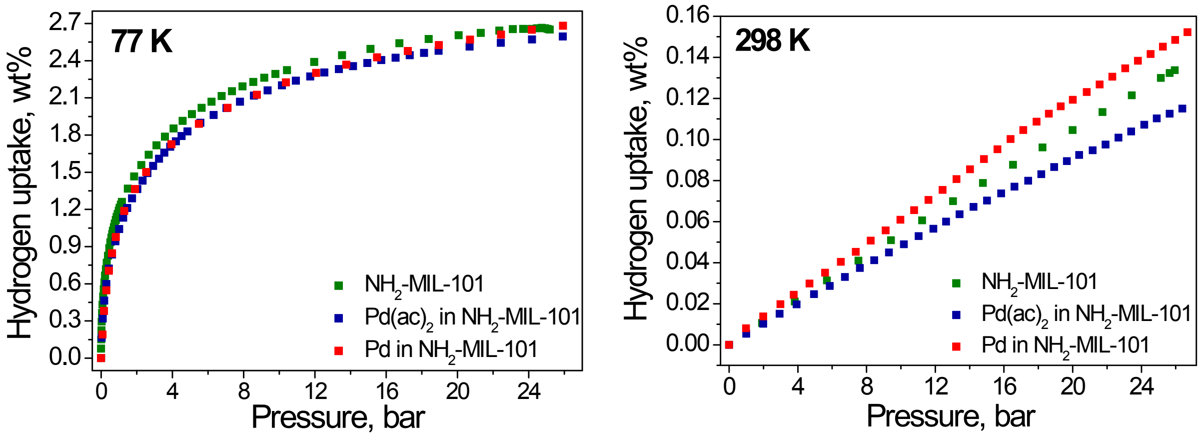

Figure S5 Hydrogen adsorption isotherms of the empty, the Pd(ac)$_2$ precursor and the elemental Pd-supporting NH$_2$-MIL-101 at 77 (left) and 298 K (right)

Metal-organic frameworks are chemically diverse materials. Even when NH$_2$-MIL-101 does not contain any Pd guest, it has various sites where H$_2$ can be adsorbed, such as the cationic unit, the –NH$_2$ functional groups, *etc.* [20], these various adsorption sites interact with hydrogen with various strength. Therefore, when the material is exposed to hydrogen, first the most strongly bonded hydrogen molecules will be adsorbed, continued by the second strongest and so on, until at high hydrogen pressures the volume of the pores will be filled indiscriminately. In addition, at low temperatures the adsorption sites can more easily bind hydrogen and thus the sample only needs to be exposed to smaller amounts of hydrogen to achieve high hydrogen adsorption or coverage of hydrogen binding sites. It therefore follows that when the sample is only exposed to a small amount of hydrogen (high temperature, low pressure) only the most strongly binding adsorption sites will be filled with hydrogen and so the hydrogen adsorption measured will be directly proportionate with the concentration of these sites. On the other hand, at low temperatures and high pressures the hydrogen uptake will be related to the total available pore volume.

The low temperature isotherm (left) reveals no great change in the hydrogen uptake for high loadings as the available pore volume did not change considerably on account of the low (0.85 wt%) Pd loading. On the other hand, in the high-temperature, *i.e.* low hydrogen loading, part of the isotherm (right) displays and increased uptake of hydrogen upon the addition of Pd. As this increase is only observed when the Pd added is in its reduced (atomic and particular) form, it can be associated with additional, strongly binding, hydrogen adsorption sites.

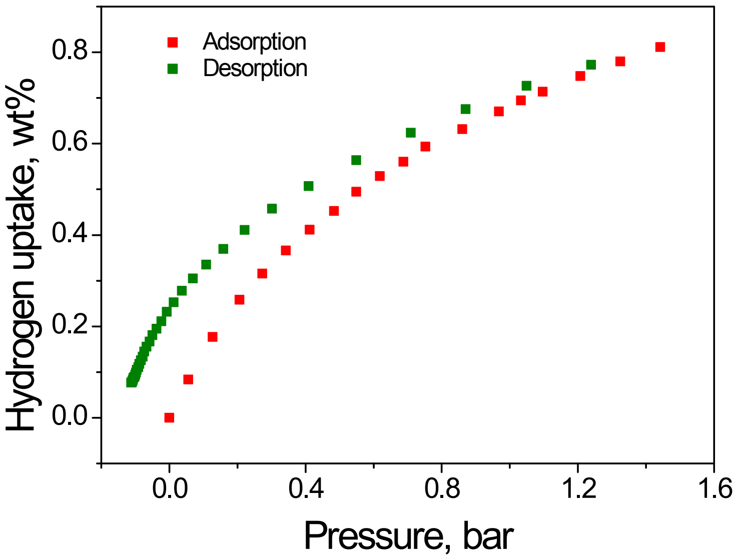

Figure S6 Hydrogen adsorption (red) and desorption (green) isotherms on 'Pd in NH_2-MIL-101(Cr)' measured at 87 K

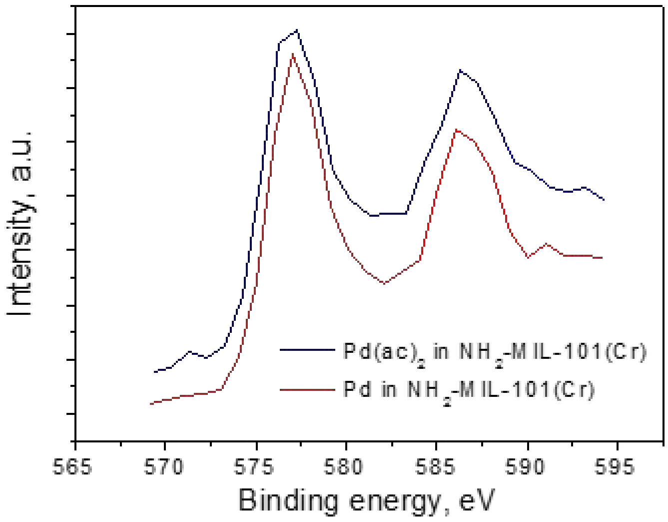

Figure S7 X-ray photoelectron spectra of the $Pd(ac)_2$ precursor (in blue) and the elemental Pd (in red) containing NH_2-MIL-101(Cr), showing no oxidation changes in the Cr^{3+} cationic unit before and after the reduction of the $Pd(NO_3)_2$ precursor at elevated temperatures in a hydrogen stream.

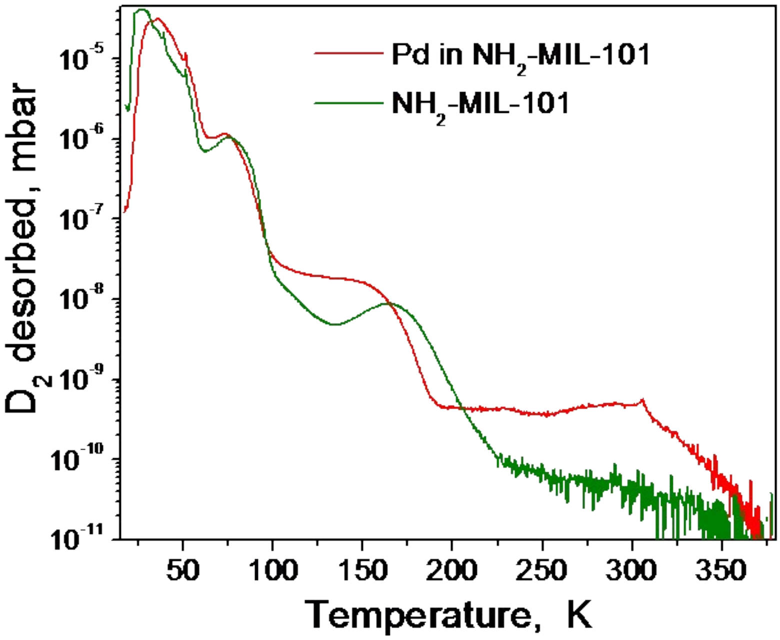

Figure S8 Temperature-programmed desorption spectra of deuterium on a semi-logarithmic scale from the pristine (green) and the Pd containing (red) NH_2-MIL-101(Cr). Note that desorption peak from the MOF CUS, which is over 20x the intensity than the 290 K peak; this is consistent with the Cr concentration being *ca.* 23x higher than that of Pd.

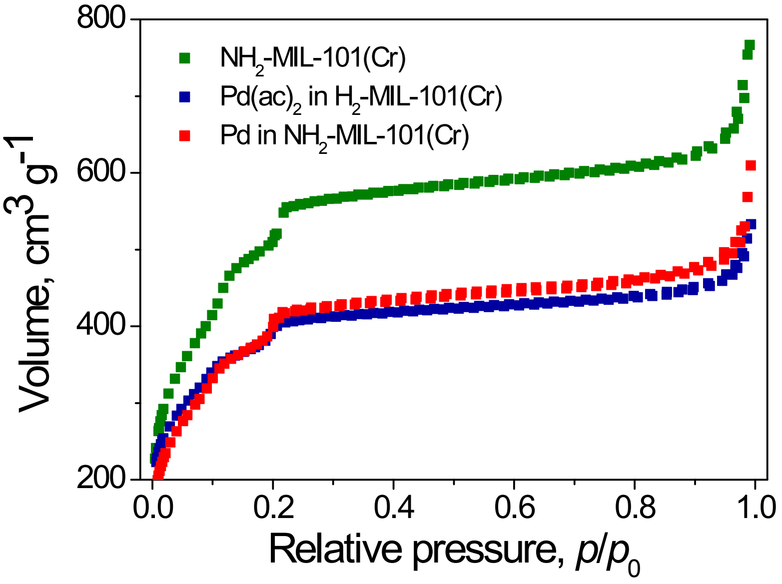

Figure S9 Nitrogen adsorption isotherms of the empty, the $Pd(ac)_2$ precursor and the elemental Pd-supporting NH_2-MIL-101 at 77 K.

Table S1 Reaction enthalpies and free energies calculated at 298K for H_2 Pd^0 and $Pd^0(NH_3)$ at the B3LYP/aug-cc-pVDZ-PP level of theory

Reaction	Structure	Enthalpy (kJ/mol)	Free energy (kJ/mol)
H_2			
Pd $(^1A_{1G})$ + H_2 $(^1\Sigma_g)$ $\rightarrow$ $Pd(H_2)$ $(^1A_1)$	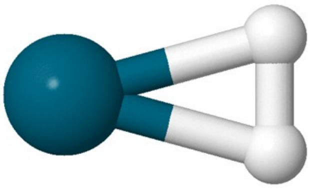	−83.32	−60.32
Pd $(^1A_{1G})$ + H_2 $(^1\Sigma_g)$ $\rightarrow$ PdH_2 $(^1A_1)$	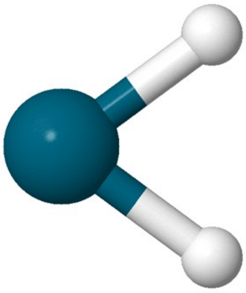	−70.55	−49.01
Pd $(^1A_{1G})$ + $Pd(H_2)$ $(^1A_1)$ $\rightarrow$ $Pd_2(H_2)$ $(^1A_1)$ (TS)	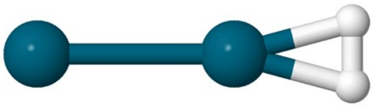	−41.72	−14.93
Pd $(^1A_{1G})$ + NH_3 $(^1A')$ $\rightarrow$ $PdNH_3$ (^1A)	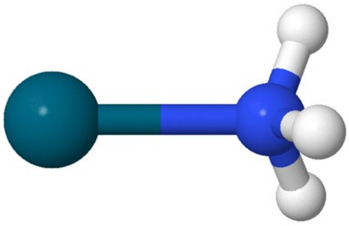	−79.68	−49.57
$PdNH_3$ (^1A) + H_2 $(^1\Sigma_g)$ $\rightarrow$ $NH_3Pd(H_2)$ (^1A) (TS)	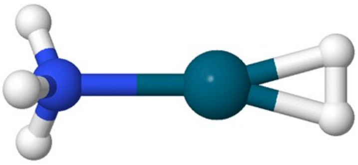	−113.00	−77.92
$Pd(H_2)$ $(^1A_1)$ + NH_3 $(^1A')$ $\rightarrow$ $NH_3Pd(H_2)$ (^1A) (TS)	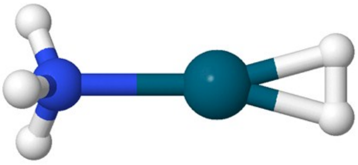	−109.35	−67.17

Table S2 Reaction enthalpies and free energies calculated at 298K for H_2 with Pd^0, Pd^I and Pd^{II}, and $Pd^0(NH_3)$, $Pd^I(NH_3)$ and $Pd^{II}(NH_3)$ at the B3LYP/6-311++G(2d,2p)/SDD level of theory

Reaction	**Structure**	**Enthalpy (kJ/mol)**	**Free energy (kJ/mol)**
	Pd 0		
Pd ($^1A_{1G}$) + 1/2H$_2$ ($^1\Sigma_g$) $\rightarrow$ PdH ($^2\Sigma$)	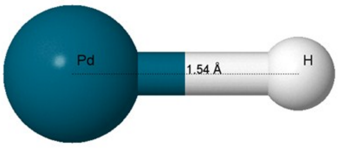	−14.66	−7.83
Pd ($^1A_{1G}$) + H$_2$ ($^1\Sigma_g$) $\rightarrow$ Pd(H$_2$) ($^1A_1$)	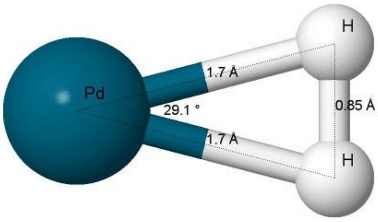	−72.33	−49.44
Pd ($^1A_{1G}$) + H$_2$ ($^1\Sigma_g$) $\rightarrow$ PdH$_2$ ($^1A_1$)	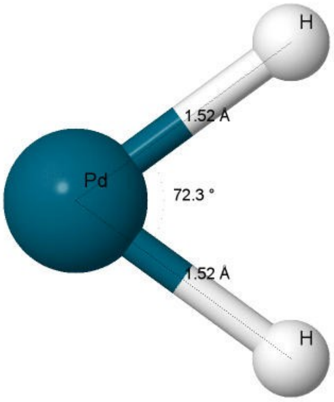	−54.50	−33.04
Pd ($^1A_{1G}$) + Pd(H$_2$) ($^1A_1$) $\rightarrow$ Pd$_2$(H$_2$) ($^1A_1$) (TS)		−39.95	−12.07
Pd ($^1A_{1G}$) + Pd(H$_2$) ($^1A_1$) $\rightarrow$ Pd$_2$H$_2$ (^1A_G)	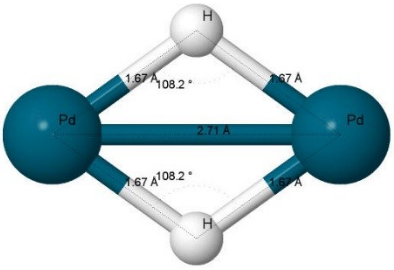	−173.42	−142.82
Pd$_2$ ($^3\Sigma_u$) + H$_2$ ($^1\Sigma_g$) $\rightarrow$ Pd$_2$(H$_2$) ($^3A_1$)	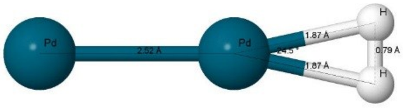	−24.74	4.23

Pd(H_2) ($^1A_1$) + H_2 ($^1\Sigma_g$) → Pd$(H_2)_2$ ($^1A_1$)	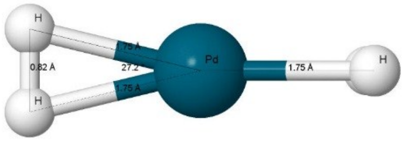	–65.71	–33.05
Pd(H_2) ($^1A_1$) + 2H_2 ($^1\Sigma_g$) → Pd$(H_2)_3$ ($^1A_1$)	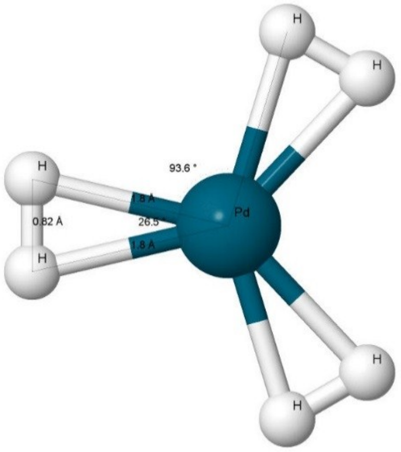	–86.81	–23.68
Pd ($^1A_{1G}$) + H_2 ($^1\Sigma_g$) → PdH_2 ($^1\Sigma$) (***1a***) (TS)	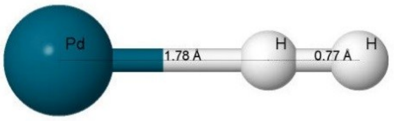	–30.22	–6.21
Pd ($^1A_{1G}$) + H_2 ($^1\Sigma_g$) → PdH_2 ($^1\Sigma_g$) (***1b***)	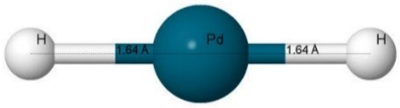	142.98	170.30
PdH ($^2\Sigma$) + H_2 ($^1\Sigma_g$) → PdH(H_2) ($^2A_1$)	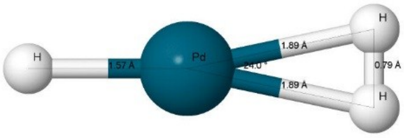	–32.55	–1.63
Pd_2 ($^3\Sigma_u$) + 1/2H_2 ($^1\Sigma_g$) → Pd_2H ($^2A'$)	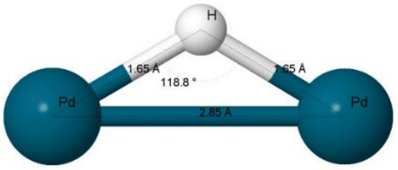	–56.45	–45.26
Pd ($^1A_{1G}$) + NH_3 ($^1A'$) → PdNH_3 (^1A)	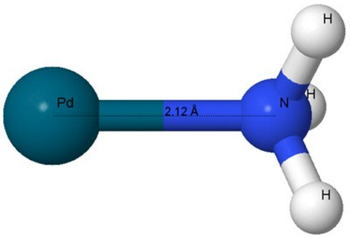	–74.96	–44.83
PdNH_3 (^1A) + H_2 ($^1\Sigma_g$) → NH_3Pd(H_2) (^1A) (TS)	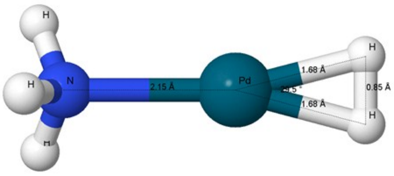	–102.19	–67.57

$Pd(H_2)\ (^1A_1) + NH_3\ (^1A') \rightarrow NH_3Pd(H_2)\ (^1A)$ (TS)		104.82	62.96
Pd I			
$Pd^{1+}\ (^2A) + H_2\ (^1\Sigma_g) \rightarrow Pd^{1+}(H_2)\ (^2A_1)$	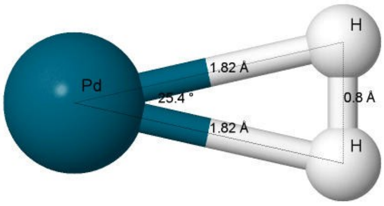	–81.13	–58.56
$Pd^{1+}\ (^2A) + H_2\ (^1\Sigma_g) \rightarrow Pd^{1+}(H_2)\ (^2A_2)$	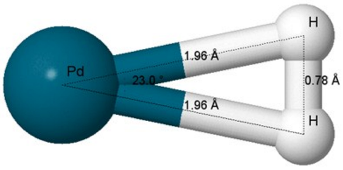	–48.86	–27.01
Pd II			
$Pd^{2+}\ (^3A_{1G}) + 1/2H_2\ (^1\Sigma_g) \rightarrow Pd^{2+}(H)\ (^2\Sigma)$	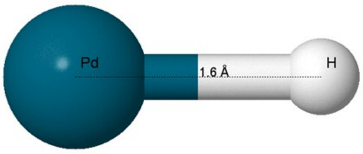	–36.94	–27.59
$Pd^{2+}\ (^3A_{1G}) + H_2\ (^1\Sigma_g) \rightarrow Pd^{2+}(H_2)\ (^1A_1)$	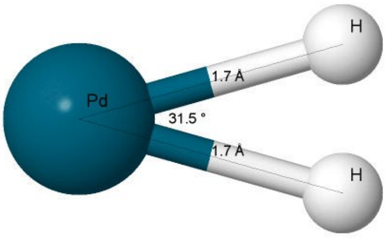	–107.92	–82.42
$Pd^{2+}\ (^1A_{1G}) + 1/2H_2\ (^1\Sigma_g) \rightarrow Pd^{2+}(H)\ (^2\Sigma)$	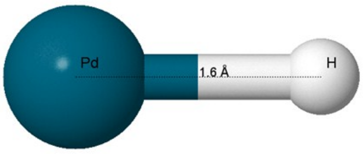	–272.55	–265.93
$Pd^{2+}\ (^1A_{1G}) + H_2\ (^1\Sigma_g) \rightarrow Pd^{2+}(H_2)\ (^1A_1)$	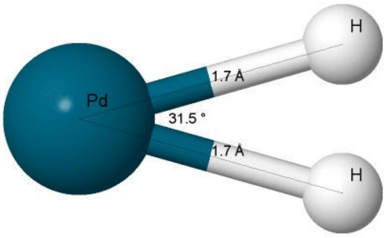	–343.54	–320.76

Electronic states in parentheses. TS in parentheses denote a transition state structure. Isolated Pd 0 is considered as a singlet and is [Kr]$5s^0 4d^{10}$. ***1a*** in parenthesis denotes reaction to linear PdHH; ***1b*** denotes reaction to linear HPdH.

Table S3 Reaction enthalpies and free energies calculated at 298K for H_2 with Pd 0 at the CCSD/6-311++G(2d,2p)/SDD level of theory

Reaction	Enthalpy (kJ/mol)	Free energy (kJ/mol)
Pd 0		
Pd ($^1A_{1G}$) + 1/2H_2 ($^1\Sigma_g$) $\rightarrow$ PdH ($^2\Sigma$)	−11.58	−4.76
Pd ($^1A_{1G}$) + H_2 ($^1\Sigma_g$) $\rightarrow$ Pd(H_2) ($^1A_1$)	−68.51	−45.53
Pd ($^1A_{1G}$) + H_2 ($^1\Sigma_g$) $\rightarrow$ PdH_2 ($^1A_1$)	−56.14	−34.45
Pd ($^1A_{1G}$) + Pd(H_2) ($^1A_1$) $\rightarrow$ Pd_2H_2 (^1A_G)	−175.02	−142.79

Electronic states in parentheses. Isolated Pd 0 is considered as a singlet and is [Kr]$5s^0 4d^{10}$.

Table S4 Total energies and predicted harmonic vibrational frequencies for the complexes of H_2 with Pd 0 calculated at the B3LYP/aug-cc-pVDZ-PP level of theory

Species	Energy (Hartrees)	Frequencies (cm^{-1})
H_2		
Pd(H_2) ($^1A_1$)	−128.6973098	1028, 1513, 2777
PdH_2 ($^1A_1$)	−128.6914703	530, 2089, 2197
$Pd_2(H_2)$ ($^1A_1$) (TS)	−256.2039392	163*i*, 55, 118, 974, 1491, 2835
$PdNH_3$ (^1A)	−184.0938796	357, 498, 498, 1092, 1617, 1618, 3459, 3572, 3572
$NH_3Pd(H_2)$ (^1A) (TS)	−185.3131587	18*i*, 271$^\#$, 319$^\#$, 373, 524, 554, 1140, 1167, 1623, 1624, 1681, 2831, 3460*, 3573, 3573

i denotes an imaginary frequency; # denotes that the mode is IR active only; * denotes that the mode is Raman active only. Electronic spin states in parentheses.

Table S5 Total energies and predicted harmonic vibrational frequencies for the complexes of H_2 with Pd 0, Pd I and Pd II calculated at the B3LYP/6-311++G(2d,2p)/SDD level of theory

Species	Energy (Hartrees)	Frequencies (cm^{-1})
Pd 0		
PdH ($^2\Sigma$)	−128.4808125	2015
Pd(H_2) ($^1A_1$)	−129.0943219	1005, 1444, 2949
PdH_2 ($^1A_1$)	−129.0864029	529*, 2099, 2204
$Pd_2(H_2)$ ($^1A_1$) (TS)	−256.9954222	148*i*, 86, 118, 947, 1413, 3010
Pd_2H_2 (^1A_G)	−257.0463077	170$^\#$, 199*, 1234*, 1277$^\#$, 1361$^\#$, 1487*
$Pd_2(H_2)$ ($^3A_1$)	−256.9966921	200, 219, 223, 713, 1093, 3632

$Pd(H_2)_2$ ($^1A_1$)	−130.3032017	253$^{\#}$, 253$^{\#}$, 541*, 897, 1086*, 1409, 1409, 3276*, 3296
$Pd(H_2)_3$ ($^1A_1$)	−131.4931625	327, 330, 362$^{\#}$, 435*, 445*, 482*, 825, 825, 955*, 1268, 1342, 1346, 3251, 3263, 3288
PdH_2 ($^1\Sigma$) (***1a***) (TS)	−129.0759822	527*i*, 527*i*, 657, 3899
PdH_2 ($^1\Sigma_g$) (***1b***)	−129.0121613	965$^{\#}$, 965$^{\#}$, 1645$^{\#}$, 1943*
$PdH(H_2)$ ($^2A_1$)	−129.6761619	327, 330, 362$^{\#}$, 435*, 445*, 482, 825, 825, 955*, 1268, 1342, 1346, 3251, 3263, 3288
Pd_2H ($^2A'$)	−256.4165948	111, 1147, 1379
$PdNH_3$ (^1A)	−184.5027192	353, 512, 515, 1110, 1659, 1659, 3486, 3588, 3588
$NH_3Pd(H_2)$ (^1A) (TS)	−185.7237574	90*i*, 258$^{\#}$, 297, 365, 538, 558, 1136, 1157$^{\#}$, 1644, 1663, 1664, 2944, 3485*, 3586, 3587
Pd I		
$Pd^{1+}(H_2)$ ($^2A_1$)	−128.7786724	871, 1275, 3573
$Pd^{1+}(H_2)$ ($^2A_2$)	−128.7656992	660, 872, 3837
Pd II		
$Pd^{2+}(H)$ ($^2\Sigma$)	−127.4472855	1431
$Pd^{2+}(H_2)$ ($^1A_1$)	−128.0665068	1170, 1405, 2529

i denotes an imaginary frequency; $^{\#}$ denotes that the mode is IR active only; * denotes that the mode is Raman active only. Electronic states in parentheses. ***1a*** in parenthesis denotes reaction to linear PdHH; ***1b*** denotes reaction to linear HPdH.

Table S6 Total energies and predicted harmonic vibrational frequencies for the complexes of H_2 with Pd 0 calculated at the CCSD/6-311++G(2d,2p)/SDD level of theory

Species	Energy (Hartrees)	Frequencies (cm^{-1})
Pd 0		
PdH ($^2\Sigma$)	−127.7332857	1983
$Pd(H_2)$ ($^1A_1$)	−128.3422766	1021, 1524, 2967
PdH_2 ($^1A_1$)	−128.3362855	607, 2101, 2191
Pd_2H_2 (^1A_G)	−255.5536126	216, 316, 1277, 1367, 1464, 1508

Electronic states in parentheses. No Raman activities are available at this level of theory in the version of Gaussian 09 employed.

Table S7 Optimised Cartesian coordinates and total energies (Hartrees) for the complexes of H_2 with Pd using B3LYP/aug-cc-pVDZ-PP

Centre number	Atomic number	Atomic type	*x*, Å	*y*, Å	*z*, Å
$Pd(H_2)$ ($^1A_1$) -128.6973098					
1	46	0	0.000000	0.000000	0.067446
2	1	0	0.000000	0.442655	-1.551256
3	1	0	0.000000	-0.442655	-1.551256
PdH_2 ($^1A_1$) -128.6914703					
1	46	0	0.000000	0.000000	0.051015

2	1	0	0.000000	0.904064	-1.173340
3	1	0	0.000000	-0.904064	-1.173340
$Pd_2(H_2)$ ($^1A_1$) (TS) -256.2039392					
1	46	0	0.000000	0.000000	-1.303275
2	1	0	0.000000	0.438417	-2.937594
3	1	0	0.000000	-0.438417	-2.937594
4	46	0	0.000000	0.000000	1.430997
$PdNH_3$ (^1A) -184.0938796					
1	46	0	0.402873	0.000036	-0.000533
2	7	0	-1.745838	0.001493	-0.001920
3	1	0	-2.126704	-0.782473	-0.562931
4	1	0	-2.057679	-0.115445	0.971505
5	1	0	-2.126903	0.885820	-0.370620
$NH_3Pd(H_2)$ (1A) (TS) -185.3131587					
1	46	0	0.332465	-0.000044	0.000259
2	1	0	1.934516	0.440129	-0.001768
3	1	0	1.934598	-0.439667	-0.001705
4	1	0	-1.805843	-0.000223	0.000976
5	7	0	-2.165881	0.851737	-0.425257
6	1	0	-2.169013	-0.787423	-0.533346
7	1	0	-2.186708	-0.061199	0.943331